Intergallery Living Polymerization Using Silicate-Anchored Photoiniferter. A Versatile Preparatory Method for Exfoliated Silicate Nanocomposites

Jianbo Di and Dotsevi Y. Sogah*

Department of Chemistry and Chemical Biology, Baker Laboratory, Cornell University, Ithaca, New York 14853-1301

Received January 30, 2004; Revised Manuscript Received December 20, 2005

ABSTRACT: Living free radical polymerization of a variety of monomers using dithiocarbamate photoiniferter modified silicate gave dispersed polymer/silicate nanocomposites, even for nanocomposites with very high silicate contents (7−63 wt %). Thus, nanocomposites containing polystyrene, poly(methyl methacrylate), poly(*tert*-butyl methacrylate), and poly(methyl methacrylate-*b*-styrene) of controlled molecular weight, architecture, and polydispersity were prepared. Dispersion and random orientation of the silicate layers in the polymer matrix were confirmed by both wide-angle X-ray diffraction and transmission (TEM) and scanning transmission electron microscopy (STEM). One principal finding is that exfoliated nanocomposites with very high silicate contents (above 20 wt %) could be used as nanoadditives or masterbatches to prepare all kinds of nanocomposites by simple blending without always having to begin from scratch. The exfoliation remained stable to subsequent thermal processing. The storage modulus of PMMA/silicate nanocomposite at only 3.2 wt % silicate loading was 30−40% higher than that of neat PMMA at all temperatures in the glassy region below the T_g of PMMA. The method is versatile, simple, and applicable to many monomers and requires no additional catalyst.

Introduction

In the production of modern plastics, enhancement of properties of polymeric materials through reinforcement with inorganic fibers, or particles of micron or greater dimensions, is common. By contrast, polymer/layered silicate nanocomposites represent a considerable advance over conventional composites.[1] Nanocomposites containing layered silicates of ultrafine phase dimensions and high aspect ratios exhibit improved and new properties compared to corresponding micro- and macrocomposites and the unfilled polymer. Significant improvements in modulus,[1−6] thermal stability,[7] heat distortion temperature,[7] barrier properties,[8−12] fire retardancy,[13−17] and other properties such as dimensional stability, surface hardness, and mar resistance have been demonstrated for various nanocomposites. In contrast to traditional composites, nanocomposites provide the improvements at a very low silicate loading, usually below 5 wt %. They offer potential for applications in tough and heat-resistant materials,[13] coatings,[18] electronics,[18] catalysis,[19] packaging,[2b] and high-temperature-compatible materials and advance the study of polymers in confined domains.[2b]

Two broad classes of polymer silicate nanocomposites, namely, intercalated[1,2,17,20] and exfoliated nanocomposites,[1,13,21,22] have been reported. In the intercalated nanocomposites, the polymer chains penetrate into the galleries between the silicate layers in a crystallographic regular fashion regardless of silicate-to-polymer ratio. The distance between the layers (*d* spacing) usually increases, but the registry of the stacking is well maintained. In the case of exfoliated nanocomposites, all the silicate layers are delaminated into single layers and randomly dispersed in the polymer matrix. The silicate content of an exfoliated nanocomposite is usually lower than that in an intercalated nanocomposite. In practice, a mixture of the two is often observed.[1]

* Corresponding author. E-mail: dys2@cornell.edu.

The property improvement observed for nanocomposites has been attributed in part to the large interface areas between the inorganic component and the polymer matrix and partly to the high aspect ratio of the silicate, both of which will increase after exfoliation of the layers. The thickness of a single silicate layer is about 1−2 nm while the length can vary from 100 nm to tens of microns, making its aspect ratio very high, which could lead to increased stiffness and strength. In addition, optical clarity will be better in the exfoliated system than in cases where the silicates remain as clusters. Hence, better property improvements are expected for the exfoliated nanocomposites. In fact, incomplete exfoliation has been shown to lead to a less effective reinforcement. Using a three-dimensional lattice spring model, Balazs et al. examined the mechanical properties of nanocomposites and attributed increased reinforcement efficiency in nanocomposites to platelet exfoliation.[23,24] In retrospect, one could regard the seminal work of the Toyota group, who prepared exfoliated nylon-6/layered silicate nanocomposite that has since been commercialized, as an experimental demonstration of the fact that exfoliated nanocomposites offer better improvement in properties.[1,12,13] Their material was prepared by in situ intercalative ring-opening polymerization of ϵ-caprolactam using MMT that was modified with α,ω-amino acids and swollen by monomer.

The Toyota results sparked intensive efforts by many research groups to develop synthetic methods for the exfoliated nanocomposites.[1] Dispersion from solution, emulsion polymerization, melt dispersion, and in situ polymerization in the presence of either reactive or nonreactive surfactant-modified silicates have all been tried to achieve exfoliated nanocomposites, albeit with varied success.[1,21,22] In addition, all the methods were system-specific; i.e., they only worked for one particular polymer or required a particular surfactant, and the nanocomposites obtained were mostly a mixture of both intercalated and partially exfoliated structures. In contrast to the paucity of reproducible methods for the synthesis of completely exfoliated polymer/

10.1021/ma049794i CCC: $33.50
Published on Web 01/24/2006

layered silicate nanocomposites, the methods for preparing intercalated nanocomposites are very well established.[1,2,25−29] Giannelis and co-workers introduced the simple melt processing technique that worked very well for many systems.[2,20] Others have used intercalation from solution or in situ polymerization of silicate-swollen monomers.[25]

The goal of our nanocomposite program is to develop reliable and versatile methods that ensure and maintain the random dispersion of the single silicate layers and, simultaneously, provide more control over the polymer architecture, such as forming block copolymers and facilitating controlled functionalization. The best way to achieve such a control is by using living polymerization methods.[30] We hypothesized that complete exfoliation would result if an appropriately designed initiator was first firmly anchored in the galleries of the layered silicates, followed by intercalating the desired monomer into the galleries and then initiating the monomer polymerization inside the galleries, because the process would give a system in which one end of the polymer chain was strongly anchored to the silicate layers. We first reported this concept of intergallery initiation from an anchored initiator in 1999.[31] In that work, we demonstrated that in situ alkoxyamine (or nitroxide)-mediated living radical polymerization from silicate-anchored initiators was very effective in producing exfoliated polystyrene/layered silicate nanocomposites. This intergallery living polymerization method did not only ensure the exfoliation of the silicate layers but also afforded the opportunity for a better control over the polymer structure. Both the molecular weight and molecular weight distribution were well controlled. More importantly, all the polymer chains in the nanocomposite were attached to the silicate layers by strong electrostatic interactions. This helped maintain the dispersion during subsequent processing and, in principle, should facilitate load transfer from the polymer matrix to the silicate layers, leading to improvements in the mechanical properties of the material. The importance of end-functionalized polymer chains in maintaining exfoliation was later confirmed theoretically by Balazs and co-workers, who found that as the attractive interaction between the functional group and clay surface increased, the system exhibited isotropic morphology, corresponding to the thermodynamically stable, exfoliated nanocomposites, at relatively low clay volume fractions.[32]

There are other examples in the literature that suggest exfoliated nanocomposites could form as a result of strong interactions between the polymer's terminal functional group and the silicate. The synthesis of exfoliated nylon-6/layered silicate nanocomposite by the Toyota group mentioned earlier is one example. Other research groups have since utilized the concept of intergallery polymerization with different initiators and polymerization methods to prepare several polymer/layered silicate nanocomposites. Mays et al. reported the preparation of PS/silicate nanocomposites by in situ living anionic polymerization from silicate anchored initiators.[33] However, they had to resort to a special apparatus because of the high sensitivity of the anionic polymerization to moisture and minute impurities. In addition, the nanocomposites they obtained contained unattached chains that had to be removed by exhaustive extraction. Giannelis et al. reported the preparation of poly(caprolactone)/silicate nanocomposite by anionic ring-opening polymerization of ϵ-caprolactone initiated by aminolauric acid anchored to MMT.[34] Dubois et al. also reported the preparation of poly(caprolactone)/silicate nanocomposites by anionic ring-opening polymerization from silicate-anchored hydroxyl groups.[35−38]

It follows that intergallery initiation from an anchored initiator has a good probability of providing an exfoliated nanocomposite. As stated earlier, obtaining polymers of controlled architectures in the nanocomposite and ensuring that each polymer chain carries the interacting end functional group are best accomplished by living polymerization methods. Unfortunately, many living polymerizations, such as anionic, cationic, and group transfer polymerizations, are sensitive to moisture and minute impurities and, therefore, are difficult to perform in the presence of silicates, especially the naturally occurring clays, which typically contain waters of hydration and trace impurities.

Of all the polymerization methods available, free radical polymerization is unarguably the most versatile for the following reasons: First, free radical polymerization is more tolerant of moisture, air, and some impurities and is therefore more compatible with the hydrophilic interior of layered silicates whose adsorbed water is difficult to remove by drying without altering the silicate structure significantly. In fact, Mays's work on anionic polymerization illustrates beautifully the difficulty involved in employing moisture-sensitive initiators.[33] Second, free radical polymerization is applicable to such a broad spectrum of monomers that its utilization in the science of nanocomposites will make available a large variety of polymer/silicate nanocomposites.

There are many elegant living/controlled radical polymerization methods to choose from.[39] As stated earlier, our published work showed that the use of silicate-anchored alkoxyamines (nitroxyl derivatives) as the intergallery polymerization initiators worked fine in demonstrating the concept and preparing PS/silicate nanocomposites.[32] However, the method has limited monomer scope. For example, it works very well for styrene and acrylate monomers but not as well for methyl methacrylate homopolymerization.[39a,b] ATRP,[39c,d] which has a wider monomer scope, has the intrinsic problem of copper impurity in the final product in addition to the amine complexing agent that could potentially interact strongly with the silicate surface. Although there are reports on removing most of the Cu from polymers, it is not obvious to us as to how Cu could be removed from the other inorganic components of the nanocomposites. Nevertheless, other research groups have made efforts to use ATRP in nanocomposite synthesis. Hallensleben and co-workers were the first to report on the preparation of PS/silicate nanocomposite using ATRP.[40a] The published XRD of their nanocomposite showed no peaks, but they did not provide any other data such as TEM to confirm complete exfoliation. After this paper was submitted, reviewed, and was being revised, a paper from Shipp and co-workers appeared that reported the use of ATRP to prepare nanocomposites containing polystyrene, methyl methacrylate, and butyl acrylate.[40b,c] In all cases, the clay particles were not completely exfoliated as evidenced by the presence of large aggregated particles in their TEM images although XRD of their products showed no diffraction peaks. Most recently, Li et al.[40e] reported the use of ATRP in the preparation of PS/silicate nanocomposite using initiator-modified magadiite. They found, as did Shipp and co-workers, that whereas the XRD showed no peak, the TEM revealed a mixture of intercalated and exfoliated nanocomposite.

Reversible addition fragmentation chain transfer (RAFT), another excellent living/controlled radical polymerization, seems promising.[39e,f] However, this polymerization requires a co-initiator, such as BPO and AIBN, in addition to the chain transfer agent, which would result in some of chains being unanchored to the silicate layers. In addition, the mechanism of RAFT requires that the growing polymeric radical intercalates

into the silicate layers in order to undergo transfer to the tethered dithioester. Very recently and while this paper was in review, Shipp and co-workers reported that they have prepared nanocomposites using RAFT.[41] Although exfoliated morphology was realized in cases where polymerizable surfactants were used to modify the clay, the observation was not general as some systems still gave mixed morphologies.

Our goal is to use a method that would minimize the number of unattached chains as much as possible and have a broad monomer scope. Hence, we selected the RAFT-related method that uses dithiocarbamates as photoiniferters. Although the sulfur-centered dithiocarbamate radical that forms upon dissociation of the photoiniferter could also initiate chain growth leading to formation of unattached polymer chains, this can be overcome through the appropriate design of the photoiniferter. For example, use of benzyl dithiocarbamate should generate a benzyl radical with which the sulfur-centered dithiocarbamate radical will not be competitive as an initiator. The main reaction that could lead to unattached chains is chain transfer to either solvent or other impurities. However, this would be true for all free radical methods.

The use of dithiocarbamates as photoinitiators started as early as 1956,[42a] but it was not until 1982 when Otsu et al.[42b,c] developed the concept of using them as what he termed "pseudo living free radical" photoiniferters. Since then, the method has led to the synthesis of various monofunctional, telechelic, block, graft, star, and cross-linked polymers.[42d] The photoiniferter method is applicable to a wide scope of monomers, having been used in the preparation of polymers of styrene, *p*-chlorostyrene, *p*-methoxystyrene, methyl methacrylate, ethyl methacrylate, methyl acrylate, vinyl acetate, diisopropyl fumarate, isobutyl vinyl ether, and maleic anhydride.[29,30] Hence, the transplant of the method into the area of polymer/silicate nanocomposites will greatly expand the scope of nanocomposites.

In this paper, we report our preliminary results on the preparation of exfoliated polymer/silicate nanocomposites by in situ polymerization from a silicate-anchored photoiniferter. The method worked reproducibly and is capable of producing nanocomposites of a broad range of silicate loading and polymer molecular weights. Taking advantage of the living characteristic of the process, we also prepared block copolymer/silicate nanocomposites by sequential monomer addition. One principal finding is that exfoliated nanocomposites with very high silicate contents (above 20 wt %) could readily be prepared. This is significant since it will allow the high silicate containing nanocomposites to be used as masterbatches in preparing all kinds of nanocomposites by simple blending without always having to begin from scratch.

Experimental Section

Materials. Sodium *N*,*N*-diethyldithiocarbamate trihydrate (99+%) and other common chemicals were purchased from Aldrich and used without any further purification, unless otherwise noted. 4-(Bromomethyl)benzyltrimethylammonium bromide (**1**) was prepared using a literature procedure.[43] Styrene (99%) was distilled over CaH_2 under reduced pressure. Methyl methacrylate (MMA) and *tert*-butyl acrylate (*t*BA) were filtered through alumina B under nitrogen. All purified monomers were stored under N_2 over a maximum of 2 months. Tetrahydrofuran (THF) was distilled from sodium benzophenone under N_2. Na−montmorillonite (designated as silicate) with a cation exchange capacity of 92.6 mequiv/100 g was obtained from Southern Clay Products, Gonzales, TX, under the name of Cloisite NA+. A high-intensity UV lamp UVP model B-100AP was purchased from VWR.

Characterization. X-ray diffraction (XRD) analysis was performed on powder samples with a Scintag X-ray diffractometer operating in the theta−theta geometry using Cu Kα (λ = 1.54 Å) or Cr Kα (λ = 2.29 Å) radiation operated at 45 kV and 40 mA. The scanning speed and the step size used were 5°/min and 0.02°, respectively. Room temperature solution ^{1}H nuclear magnetic resonance (NMR) spectra were obtained at 400 MHz on a VXR-400S spectrometer. Samples (25 mg) were dissolved in DMSO-d_6 (1 g). Polymer molecular weights were determined by size exclusion chromatography (SEC) in THF using a Waters GPC with Ultrastyragel (Waters Associates) columns and both refractive index and UV detectors. Retention times were converted to polymer molecular weights using a calibration curve built from narrow molecular weight distribution PS standards. Thermogravimetric analyses (TGA) were carried out under N_2 on a Seiko thermogravimetric differential thermal analyzer using a heating rate of 5.0 °C/min. Scanning transmission electron microscopy (STEM) was done with a 100 keV HB501/UX dedicated scanning transmission electron microscope utilizing a cold field emission gun to produce a 2 Å probe, which is scanned over the specimen. The bright field and annular dark field images were digitally and simultaneously acquired and stored in standard TIFF format using a Microsoft Windows-95 based interactive graphical program WINSTEM. The specimen was prepared by grinding the bulk material in 2-propanol in an agate mortar. A holey carbon film on a copper washer was then swept through the 2-propanol, picking up numerous microscopic pieces of the material on the carbon film. Dynamic mechanical analysis (DMA) was performed on an injection-molded dog-bone shape of each sample using a DACA microinjector with a barrel temperature at 160 °C and mold temperature at 80 °C. The DMA of the injection-molded samples was done using a TA Instruments dynamic mechanical analyzer DMA 2980 at a fixed frequency of 1 Hz. The temperatures studied ranged from −130 to 140 °C, with a heating rate of 3 °C/min.

Purification of the Silicate. To a 1000 mL flask equipped with a stirring bar was added MMT-Na (5.0 g). Deionized water (800 mL) was added to the flask. The mixture was stirred at room temperature for 24 h. It was left to stand for 1 week, during which solid particles settled. The upper portion of the dispersion was decanted into a round-bottom bottle and lyophilized to remove all the water to give 4.85 g (97%). In general, the amount of material discarded varied between 2 and 4 wt %.

4-(*N*,*N*-Diethyldithiocarbamylmethyl)benzyltrimethylammonium Bromide (2). To a 1000 mL flask equipped with a stirring bar were added 4-(bromomethyl)benzyltrimethylammonium bromide (**1**) (8.60 g, 26.6 mmol), sodium *N*,*N*-diethyldithiocarbamate trihydrate (12.0 g, 53.3 mmol), and acetone (200 mL). The mixture was stirred at room temperature for 24 h. A white precipitate formed gradually. The precipitate was filtered and washed with technical acetone (500 mL × 3). The white powder was dried in a vacuum oven overnight. Yield: 10.4 g (98.0%). ^{1}H NMR: δ (DMSO-d_6) 1.14−1.20 (m, 6H), 2.98 (s, 9H), 3.70−3.72 (q, 2H), 3.94−3.96 (q, 2H), 4.47 (s, 2H), 4.56 (s, 2H), 7.44−7.52 (q, 4H).

A Typical Procedure for the Preparation of Photoiniferter-Modified Silicate. To a 4 L flask equipped with a stirring bar were added photoiniferter **2** (3.69 g, 9.44 mmol) and deionized water (3 L). The solution was stirred for 5 min to dissolve the photoiniferter. To a separate 1 L beaker equipped with a stirring bar were added purified silicate (10.0 g, 9.26 mequiv) and deionized water (1 L). The silicate/water mixture was stirred for 10 min so that the silicate was well dispersed in the water. The dispersion was then added to the aqueous solution of **2** with stirring. Stirring was continued for 12 h at room temperature. After the stirring was stopped, solids settled at the bottom of the mixture within 5−10 min, and the reaction mixture was centrifuged. After removing the water, the modified silicate was washed with water several times (1 L × 3), and each time the water was removed after centrifuging. The resulting modified silicate was freeze-dried into loose fine powdery particles. No additional grinding was needed. Yield: 130 g (95%). In general, the yield varied from 86.2 to 95.0%

General Procedure for Preparation of Homopolymer Nanocomposites. To a three-neck round-bottom flask equipped with a stirring bar were added the desired amounts of photoiniferter-

Scheme 1

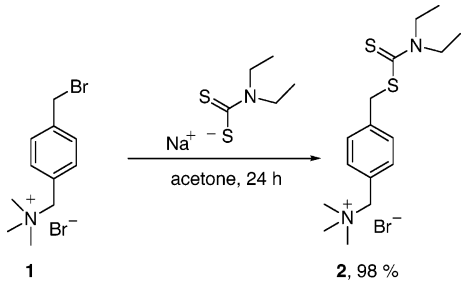

1 **2**, 98 %

modified silicate, monomer, and THF (200 mL). Nitrogen gas was bubbled into the mixture with stirring for 30 min. A UV lamp positioned 10 cm away from the flask was turned on and left on for 48 h. The temperature of the reaction flask was maintained around room temperature by the air flow in the hood. Nitrogen gas was kept on throughout the whole process. At the end of the polymerization, the UV lamp was turned off and the mixture diluted with THF (~150 mL). The product was precipitated into methanol (10-fold excess). The white solid was filtered and dried in a vacuum oven. Yields are as indicated in the reaction Tables 1−3 (see text).

The above purification procedure was used for PS and PMMA. For poly(*tert*-butyl acrylate) (P*t*BA), the polymer/THF mixture was kept under vacuum for 24 h to remove all the solvent and any unreacted monomer. The resulting yellowish solid was ground into powder while being cooled in liquid nitrogen.

Preparation of Poly(styrene-*b*-methyl methacrylate)/Silicate Nanocomposite. To a three-neck round-bottom flask equipped with a stirring bar were added Sil-PS nanocomposite (1.00 g) prepared by the preceding procedure, MMA (5.50 mL), and THF (100 mL). The mixture was degassed by bubbling nitrogen gas through it with stirring for 30 min. A UV lamp positioned 10 cm away from the flask was turned on and left on for 48 h at room temperature. Nitrogen gas was kept on throughout the whole process. At the end of the polymerization, the UV lamp was turned off and the product was precipitated into methanol (10-fold excess). The white solid was filtered and dried in a vacuum oven to give Sil-PS-*b*-PMMA in 65.5% yield. The procedure was repeated using Sil-PMMA (1.0 g), styrene (5.50 mL), and THF (100 mL) to give Sil-PMMA-*b*-PS nanocomposite in 43.2% yield.

Reverse Cation Exchange. The nanocomposite (1.0 g) was dissolved in THF (50 mL), and LiBr (0.05 g) was added to the solution. The mixture was refluxed under N_2 for 24 h. The solution was filtered through Celite. The filtrate was poured into methanol (10-fold excess) to precipitate the polymer. The product was filtered and dried in a vacuum oven.

Results and Discussion

Synthesis of the Photoiniferter and Incorporation into the Layered Silicate. The desired photoiniferter must contain a photoactive initiating moiety (in this case, the benzyl dithiocarbamate) capable of effecting living/controlled free radical polymerization of a variety of monomers. For an anchoring site, we chose the benzyltrimethylammonium moiety because it cannot undergo β-H Hoffman elimination at elevated temperatures unlike most of the current surfactants used in modifying clays. Scheme 1 shows the synthesis of the photoiniferter from 4-(bromomethyl)benzyltrimethylammonium bromide (**1**). The displacement of the bromide by sodium *N*,*N*-diethyldithiocarbamate occurred in a straightforward manner to give the desired photoiniferter **2** in almost quantitative (98%) yield. The reaction was so clean that the only purification necessary was washing the precipitate with acetone and drying.

The incorporation of **2** into the silicate was achieved by simply mixing and stirring an aqueous solution of **2** in a stable dispersion of a commercially available montmorillonite (MMT)

Scheme 2. Representation of the Photoiniferter Intercalation into the Silicate Layers via Ion Exchange

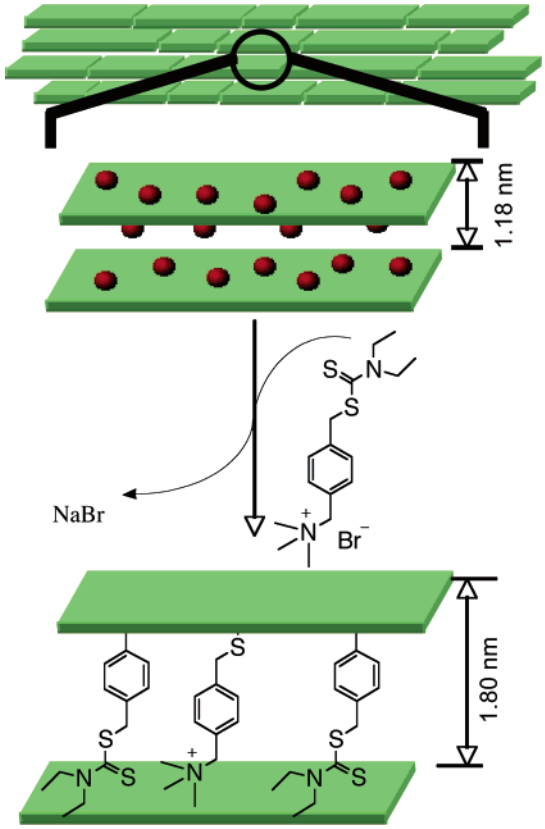

[a] The dots denote the exchangeable cations (e.g., Na^+) in the silicate galleries; plates denote the silicate layers.

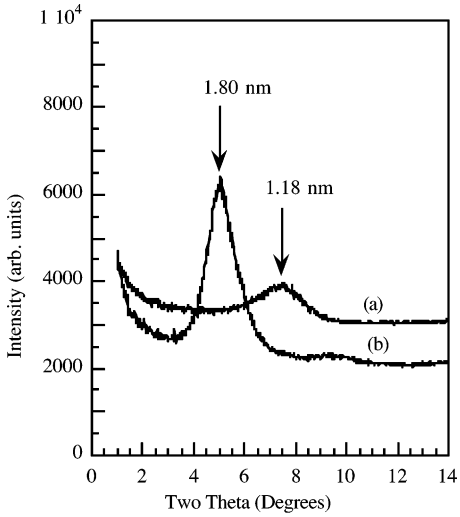

Figure 1. X-ray diffraction of (a) original silicate and (b) photoiniferter-modified silicate.

having cationic exchange capacity of 92.6 mequiv/100 g (Scheme 2).[32] The extent of the intercalation was verified by XRD and TGA measurements.

Figure 1 shows the XRD plots for the starting and the modified MMT. The original MMT had an intergallery spacing (*d* spacing) of 1.18 nm (the value provided by supplier was 1.17 nm). The product showed a *d* spacing of 1.80 nm, corresponding to an increase of 0.62 nm, which provides unambiguous evidence that the photoiniferter is inside the gallery of the silicate. TGA measurements gave the amount of the initiator in the silicate to be 0.57 mmol/g, corresponding to 62% of the full cation exchange capacity of the silicate.

Scheme 3

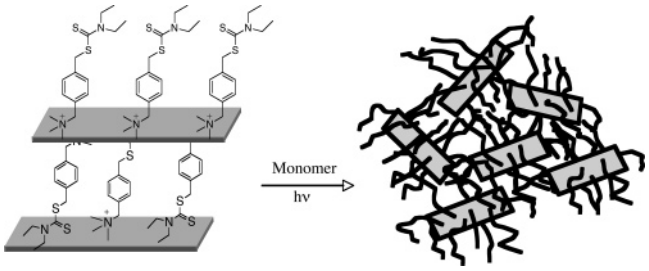

PS/Silicate Nanocomposite. The modification of the silicate layers did not only provide intergallery initiating sites but also rendered the surface of the silicate layers hydrophobic and therefore more compatible with the monomer. For the initiation to take place inside the gallery the monomer must be able to adequately wet the silicate layers.

The concept of in situ living polymerization from the silicate-anchored photoiniferter is illustrated in Scheme 3. The polymerization was carried out by simply shinning light on the stirred reaction mixture. The polymerization results are presented in Table 1. The silicate content varied from 0.7 to 62.5 wt %. To obtain information about the molecular weight of the polymers, the nanocomposite was refluxed in THF in the presence of LiBr, leading to desorption of the polymer chains from the silicate. The isolated polymer had M_n varying from 5800 to 102 000 with polydispersity index (PDI) of ca. 1.5 for lower molecular weight and 1.8−2.0 for higher molecular weight samples. As the molecular weight increased, the silicate content decreased. This is consistent with the molecular weight being controlled by the monomer/initiator ratio.

In general, the observed values of M_n were higher than calculated ones except for the polymer with the highest molecular weight. Initiation efficiencies were estimated from the ratio of observed M_n to calculated M_n and found to vary from 25% for Sil-PS-4 to 82% for Sil-PS-5. To determine the dependence of the extent of exfoliation on molecular weight, shed light on the stage at which the exfoliation occurred, and confirm that the initiation occurred inside the galleries, several runs were performed at different monomer to silicate-anchored initiator ratios.

Each reaction was monitored by XRD (Figure 2). Sample Sil-PS-1 (Figure 2b) corresponding to the lowest monomer/initiator ratio and the lowest expected molecular weight showed a peak with a *d* spacing of 1.92 nm, suggesting the formation of an intercalated nanocomposite. The M_n of the PS in that sample (Table 1) was 5800 with a silicate content of 62.5 wt %. The increase in the gallery spacing is a clear indication that the polymerization was taking place inside the galleries of the silicate layers, initially forming an intercalated structure in which the chains were still short. When the molecular weight increased to 13 600 (Sil-PS-2) and the silicate content decreased to 27.1 wt %, the sample gave no peak in its XRD (Figure 2c), indicating that the spacing between the silicate layers was no longer in registry or too large and beyond the detection limit of the instrument. This has usually been taken as an indication of the layers becoming exfoliated or disordered. Our results have been corroborated by electron microscopy (vide supra). It appears that as the polymerization inside the confined galleries progressed and both the amount and the molecular weight of the polymer inside the galleries increased, the layers were gradually pushed apart until they eventually became delaminated.

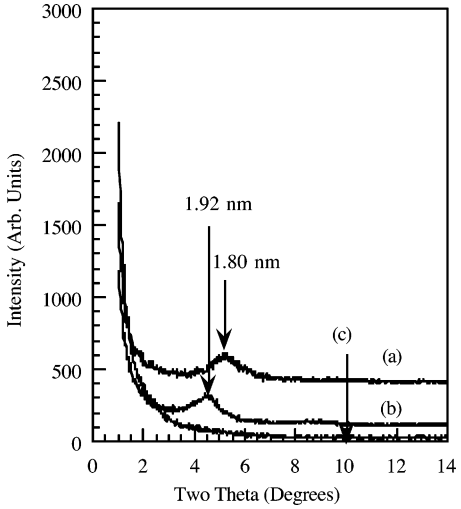

Figure 2. X-ray diffraction of (a) photoiniferter-modified silicate, (b) Sil-PS-1, and (c) Sil-PS-2.

In the examples provided, the exfoliation of the silicate layers appeared to have occurred between molecular weights of 5800 and 13 600, as evidenced by the disappearance of the XRD peaks. The XRD plots (not shown) of the remaining samples in Table 1 having silicate contents of 20.5−0.7 wt % also showed no peaks. As we have reported previously,[32] the intergallery initiation and polymerization should be distinguished from the well-known purely surface-initiated polymerization, which we pioneered in the late 1980s[44a] and was later developed by many other research groups,[44b−d] by the fact that in the latter the chains and the polymerization process are not confined in any manner. However, once exfoliation occurs, the two processes should become similar.

As stated above, the absence of Bragg diffraction peaks in the XRD of nanocomposites has been taken in many instances to indicate exfoliation of the layers. However, there are examples in the literature where XRD failed to reveal stacks of silicate layers either because the stacks are randomly dispersed or are present in only small amounts or because the spacing within the layers are beyond XRD detection limit.[45] Hence, we sought to obtain corroborative evidence from other techniques, such

Table 1. Preparation of Polystyrene/Silicate Nanocomposites

sample[a]	Sil-I[b] (g)	styrene (mL)	yield (%)	M_n ($\times 10^{-3}$) (calcd)[c]	M_n ($\times 10^{-3}$) (SEC)[d]	PDI[d]	Sil (wt %)[e]	f[f]
Sil-PS-1	3.00	15.0	30.9	2.6	5.8	1.57	62.5	0.45
Sil-PS-2	2.50	20.0	44.0	5.9	13.6	1.52	27.1	0.43
Sil-PS-3	1.70	20.0	48.1	9.5	19.0	1.54	20.5	0.50
Sil-PS-4	5.00	50.0	42.0	7.1	28.3	1.53	17.2	0.25
Sil-PS-5	0.60	40.0	30.3	34.0	41.3	1.80	7.2	0.82
Sil-PS-6	0.50	80.0	45.5	122.5	102.0	2.02	0.7	*g*

[a] Sil-PS stands for silicate/polystyrene nanocomposite. [b] Photoiniferter-modified silicate. [c] Calculated value based on monomer conversion and equivalent of initiator sites. [d] Determined by SEC in THF. [e] Determined by TGA under N_2 at a heating rate of 5.0 °C/min. [f] Initiator efficiency. [g] Cannot be determined since observed M_n is lower than calculated M_n.

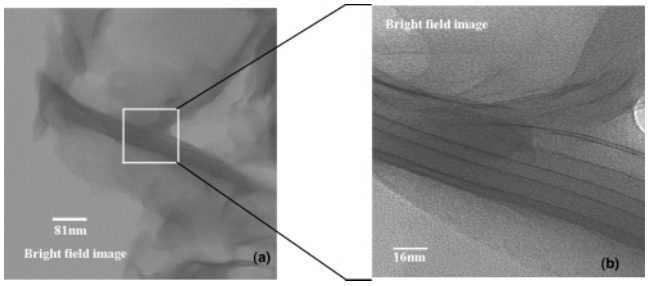

Figure 3. STEM images of Sil-PS-2. Image (b) is a higher magnification image of the marked area in image (a).

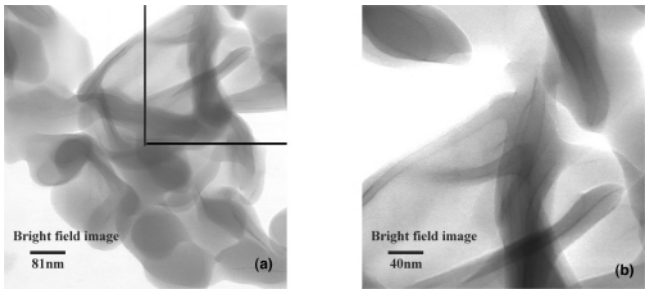

Figure 4. STEM image of Sil-PS-5. Image (b) is a higher magnification image of the marked area in image (a).

as TEM, STEM, and SEM. Figure 3 depicts the STEM image observed for the nanocomposite containing very high silicate content, typified by Sil-PS-2 (27.1 wt % silicate). The STEM revealed not only exfoliated single silicate layers with random orientations but also regions containing a stacking of 4−6 parallel silicate layers with interlayer spacings of 6−8 nm. This is another example where XRD did not detect the stacks whose layers were clearly in registry (not completely exfoliated) but had interlayer spacings beyond its detectable range. This observation reinforces the need to obtain other evidence for exfoliation besides XRD measurements, where possible. This is especially important in cases where silicate concentration in the polymer necessitates that the layers be close to one another as is the case for high silicate containing nanocomposites. As pointed out by Ray and Okamoto in their comprehensive review,[1] the average distance between the layers in exfoliated nanocomposites depends on silicate loading. The higher the silicate content, the more difficult it is to realize complete exfoliation. Further examination of the micrograph of Figure 3 revealed that the layers in these high silicate-containing materials were ∼400 nm long, suggesting edge-to-edge aggregation of two layers (the original silicate contained 100 × 200 nm layers). This type of flocculation has the effect of increasing the aspect ratio of the inorganic modifier, which could further enhance the mechanical performance of the nanocomposite. Further decrease in the silicate content led to better exfoliation. Figure 4 shows the STEM for Sil-PS-5, which had much lower silicate content, 7.2 wt %. As can be seen from the micrograph, the majority of the silicate layers observed were single layers with random orientation. The stacks of silicate layers previously observed for the high silicate-containing nanocomposite disappeared almost completely. We are not aware of any reported exfoliated nanocomposite that contained such high silicate contents as reported herein. This reinforces the notion that in situ living polymerization from silicate-anchored initiators producing silicate-anchored chains is a reliable and effective method for preparing exfoliated silicate nanocomposites. The results also reaffirm the inferences drawn from the theoretical work of Balazs.[28,29,31] The availability of exfoliated nanocomposites of very high silicate contents will advance the "masterbatch" approach to nanocomposite preparation (vide supra).

The masterbatch approach entails using the high-silicate-containing material as an additive to prepare other nanocomposites by simple blending. The success of the approach is dependent on the layers remaining delaminated in the blend. For this to happen the chains must be firmly anchored to the silicate, which is what the in situ intergallery process using preanchored initiators is designed to accomplish. The use of the nanocomposites reported herein as masterbatches for the preparation of other nanocomposites will be subject of separate publications.

Nanocomposites Containing PMMA and P*t*BA. Both solution polymerization and bulk polymerization methods were utilized for the preparation of PMMA/silicate nanocomposites (Table 2). In all cases, the yields were over 60%. PDI varied between 1.23 and 1.73 for solution polymerization and between 1.27 and 1.46 for the bulk process. The molecular weights increased with decreasing silicate content as previously observed for polystyrene. Bulk polymerization gave a transparent solid; at comparable silicate content, it gave polymer with much higher molecular weight than did solution polymerization, indicating lower initiator efficiency in bulk polymerization. This could be because the photoiniferter-modified silicate is less wettable in MMA than in THF/MMA solution, which will make the reactive sites less accessible to monomer, leading to reduced efficiency of the initiator.

As shown in Figure 5, the XRD of the PMMA/silicate nanocomposite samples gave no peak in all cases examined, regardless of the silicate content (up to 16 wt %). The STEM of Sil-PMMA-3 (Figure 6) showed single silicate layers with random orientations, confirming the formation of exfoliated nanocomposites. Okamoto et al.[1] used organically modified smectite clays to prepare several PMMA/Clay nanocomposites. Their process also involved in situ polymerization but using unattached initiators. The XRD of the product showed a small peak while TEM revealed stacked silicate layers of about 200 nm in length and about 40−50 nm in thickness that consisted of 10 parallel individual layers that were randomly distributed. Hence, the strong electrostatic interactions between

Table 2. Preparation of PMMA/Silicate Nanocomposites

entry[a]	Sil-I[b] (g)	monomer (mL)	yield (%)	$M_n \times 10^{-3}$ (calcd)[c]	$M_n \times 10^{-3}$ (SEC)[d]	PDI[d]	Sil content (wt %)[e]
Sil-PMMA-1	4.00	30.0	73.8	9.6	48.2	1.56	15.6
Sil-PMMA-2	3.00	40.0	73.4	17.0	64.4	1.23	10.7
Sil-PMMA-3	2.70	60.0	75.6	29.0	70.4	1.73	7.5
Sil-PMMA-4[f]	4.10	40.0	72.6	12.3	96.8	1.27	12.8
Sil-PMMA-5[f]	3.00	100.0	65.5	37.8	146.9	1.46	5.6
Sil-P*t*BA-1	3.50	30.0	71.2	10.0	12.6	1.63	17.8
Sil-P*t*BA-2	2.00	20.0	65.3	10.6	18.4	1.67	12.5
Sil-P*t*BA-3	2.00	50.0	68.2	27.6	30.5	1.67	5.7

[a] Sil stands for silicate. [b] Photoiniferter-modified silicate. [c] Calculated based on monomer conversion and incorporated initiator sites. [d] Determined by SEC in THF relative to PS standards. [e] Determined by TGA under N_2 at a heating rate of 5.0 °C/min. [f] Bulk polymerization.

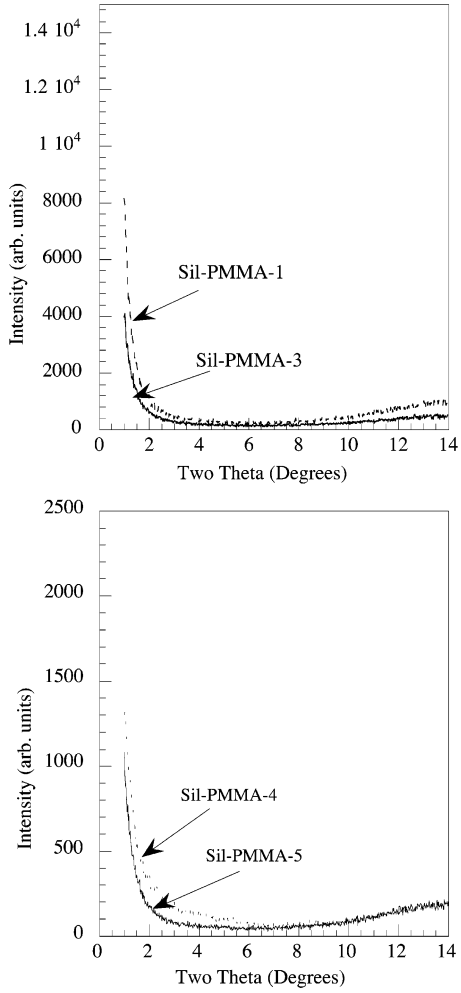

Figure 5. X-ray diffraction of PMMA nanocomposites. Designations are the same as in Table 2.

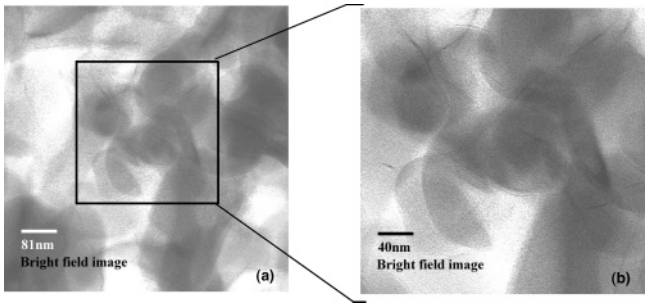

Figure 6. STEM image of Sil-PMMA-3. Image (b) is a higher magnification image of the marked area in the image (a).

the ammonium end groups of the photoiniferter and the clay layers in our example might explain the better exfoliation we observed.

The above process was extended to polyacrylates. P*t*BA/silicate nanocomposites were thus prepared, and the results are summarized in Table 2. The polymerizations gave similar results as the polymerization of MMA in terms of yield, PDI, molecular weights, and silicate contents. All the XRD (not shown) gave no peaks while STEM images (Figure 7) showed single silicate layers with random orientations, confirming the formation of exfoliated P*t*BA silicate nanocomposites.

Block Copolymer Silicate Nanocomposites. An important advantage offered by the living polymerizations is the capability to prepare nanocomposites containing block copolymers by sequential addition of monomers (Scheme 4). In the first trial,

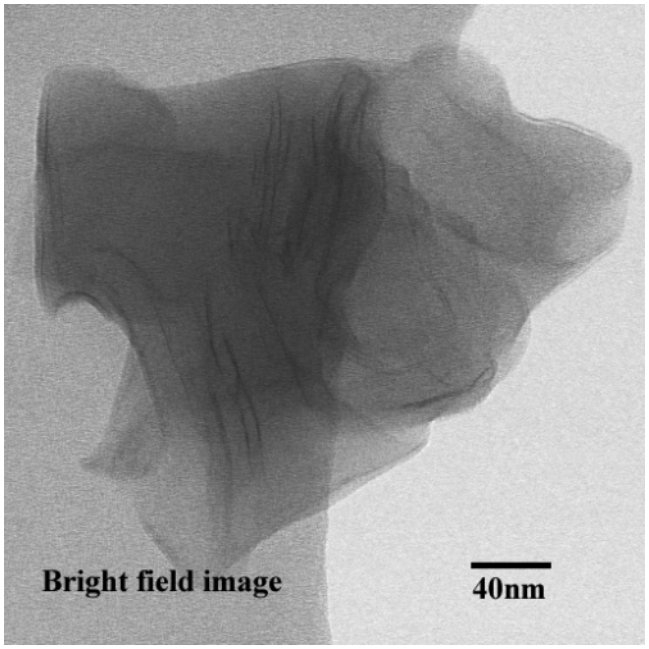

Figure 7. STEM image of Sil-P*t*BA-3 (5.7 wt % clay).

PS/silicate nanocomposite containing living PS chain ends was employed to initiate living free radical polymerization of MMA to give Sil-PS-*b*-PMMA. In a similar manner, PMMA/silicate nanocomposite was employed to initiate living free radical polymerization of styrene to obtain Sil-PMMA-*b*-PS. ^{1}H NMR spectra of both polymers showed peaks from both PS and PMMA. The curve for PS-*b*-PMMA shifted toward higher molecular weight, indicating increase in molecular weight. PDIs of both polymers were between 1.56 and 1.60. Similar observations were made in analyzing the SEC of PMMA and PMMA-*b*-PS obtained from Sil-PMMA and Sil-PMMA-*b*-PS, and the data are summarized in Table 3.

Clearly, the silicate layers that were already exfoliated in each starting homopolymer nanocomposite remained exfoliated in the block copolymer system, suggesting that no reaggregation of silicate layers occurred during the formation of the second block. This is confirmed in Figure 8 which shows the XRD curves of Sil-PS-*b*-PMMA and Sil-PMMA-*b*-PS compared to the corresponding homopolymer nanocomposites; all the curves showed no peaks, indicating that, indeed, the silicate layers remain dispersed. These observations were confirmed by TEM measurements.

Dynamic Mechanical Properties. To obtain preliminary information about the mechanical performance of the PMMA silicate nanocomposites, DMA was performed on both the nanocomposite and neat PMMA with similar molecular weight (both around 50 000). The storage modulus of the nanocomposite relative to that of neat PMMA plotted against temperature is shown in Figure 9. The storage modulus of the nanocomposite remained 30−40% higher than that of neat PMMA at all temperatures in the glassy region below the T_g of PMMA (ca. 105 °C). In the rubbery region (above the T_g) the material loses all mechanical integrity, as expected.

Demonstration of the Masterbatch Concept. Dispersion of the Silicate Layers in PS/Silicate Nanocomposite/Neat PS Blend. To demonstrate the use of high-silicate-containing nanocomposites as a masterbatch, PS/silicate nanocomposite with 20.5 wt % silicate (Sil-PS-3) was blended with neat PS in THF to give a final PS/silicate nanocomposite with 4.7 wt % silicate. The resulting nanocomposite yielded an XRD curve

Scheme 4

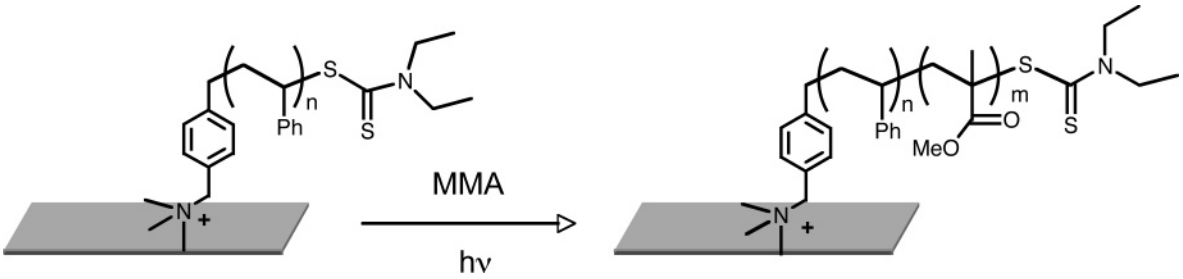

Table 3. Preparation of Block Copolymer/Silicate Nanocomposites

starting nanocomposite (g)	second monomer (mL)	yield (%)	$M_n \times 10^{-3}$ (SEC)[a]	PDI[a]
Sil-PS			11.0	1.60
Sil-PS (0.50)	MMA (20.0)	65.5	25.8	1.56
Sil-PMMA			29.1	1.43
Sil-PMMA (0.50)	styrene (20.0)	43.2	47.8	1.59

[a] Determined by SEC in THF relative to PS standards.

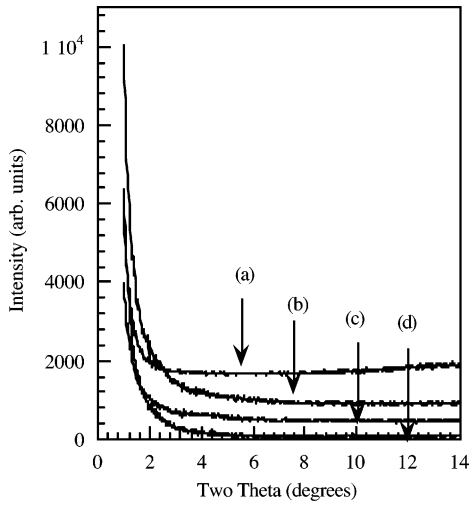

Figure 8. X-ray diffraction of block copolymer/silicate nanocomposites: (a) Sil-PS, (b) Sil-PS-*b*-PMMA, (c) Sil-PMMA, and (d) Sil-PMMA-*b*-PS.

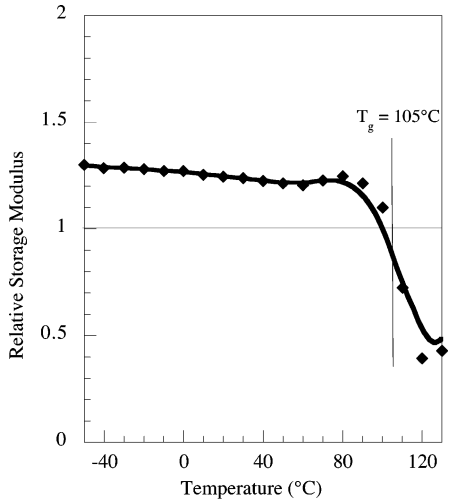

Figure 9. Relative dynamic storage modulus vs temperature plot of PMMA/silicate nanocomposite with 3.2% silicate content.

(not shown) with no diffraction peak while STEM (Figure 10) showed that the silicate was dispersed into single layers with random orientations. The bundles of layers with *d* spacing around 6−8 nm observed in the original nanocomposite (Figure 3) were absent. Since the neat PS was chemically identical to the PS in the nanocomposite additive, the two are totally miscible with each other, leading to the PS covered silicate layers being dispersed evenly in the neat PS matrix to give a fully dispersed morphology. Application of the concept to other systems such as SBS, PMMA, PE, and PP is in progress and will be the subject of a separate publication.

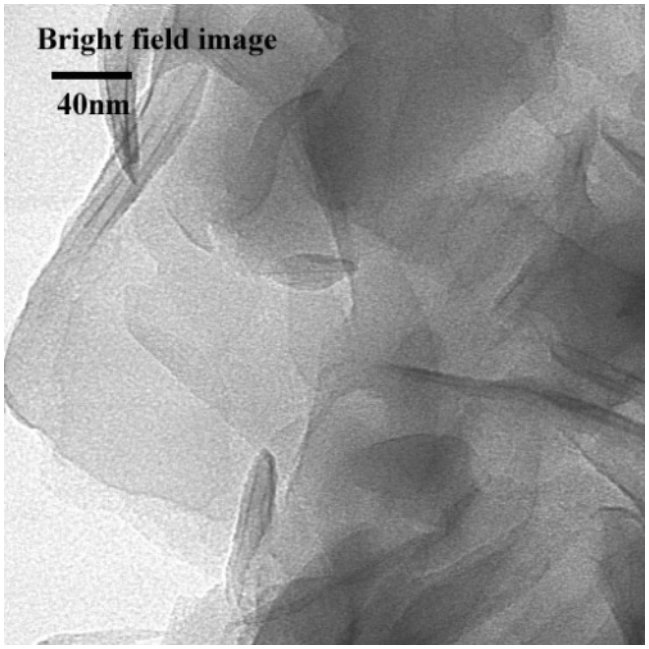

Figure 10. STEM of PS/silicate nanocomposite/neat polystyrene blend (4.7 wt % silicate overall).

Conclusions and Summary

In an effort to extend our method of direct preparation of dispersed polymer silicate nanocomposites via in situ living polymerization from silicate anchored initiators to other polymers, we have designed and prepared a dithiocarbamate photoiniferter-modified silicate. Subsequent living free radical polymerization of a variety of monomers gave dispersed polymer silicate nanocomposites. Thus, PS, PMMA, and P*t*BA/silicate nanocomposites were prepared with controlled molecular weight and PDI. Dispersion of the silicate layers in the polymer matrix was confirmed by both XRD and STEM. In all the samples prepared, the polymer chains remained attached to the silicate layers by strong ionic interactions. The PMMA/silicate nanocomposites prepared showed higher storage moduli compared with neat PMMA. Employing the technique of sequential monomer addition, polystyrene-*b*-poly(methyl methacrylate) silicate nanocomposites were prepared. Either the PS or the PMMA chain end could be attached to the silicate layers. The block structure was confirmed by SEC and NMR. XRD showed that the silicate layers were disordered in the polymer matrix.

Acknowledgment. This research was funded by NSF under Grant DMR-0079992 and DuPont Company through Polymer Outreach Program of Cornell Center for Materials Research (CCMR). Particular acknowledgment is made of the use of the XRD, STEM, SEC, TGA, and DSC Facilities of the CCMR. The STEM laboratory is supported by CCMR under Grant DMR-9632275 while the HB501 UHV-STEM was acquired through funding by the NSF (DMR-8314255). The authors thank Mr. Mick Thomas for guidance with STEM, Dr. Maura Weathers for help with XRD measurements, and Dr. Marc Weimer for help in the beginning of this work.

References and Notes

(1) Ray, S. S.; Okamoto, M. *Prog. Polym. Sci.* **2003**, *28*, 1539−1641.
(2) (a) Giannelis, E. P. *Adv. Mater.* **1996**, *8*, 29−35. (b) Wong, S.; Vaia, R.; Vasudevan, S.; Giannelis, E. P.; Zax, D. B. *J. Am. Chem. Soc.* **1995**, *117*, 7568. (c) Vaia, R. A.; Vasudevan, S.; Karwiec, W.; Scanlon, L. G.; Giannelis, E. P. *Adv. Mater.* **1995**, *7*, 154. (d) Krishnamoorti, R.; Vaia, R. A.; Giannelis, E. P. *Chem. Mater.* **1996**, *8*, 1728. (e) Giannelis, E. P.; Krishnamoorti, R.; Manias, E. *Adv. Polym. Sci.* **1999**, *138*, 107−147.
(3) Giannelis, E. P. *Appl. Organomet. Chem.* **1998**, *12*, 675−680.
(4) LaBaron, P. C.; Wang, Z.; Pannavaia, T. J. *Appl. Clay Sci.* **1999**, *15*, 11−29.
(5) Vaia, R.; Proce, G.; Ruth, P. N.; Nguyen, H. T.; Lichtenhan, J. *Appl. Clay Sci.* **1999**, *15*, 67−92.
(6) Biswas, M.; Sinha, R. S. *Adv. Polym. Sci.* **2001**, *155*, 167−221.
(7) Giannelis, E. P. *Appl. Organomet. Chem.* **1998**, *12*, 675−680.
(8) Xu, R.; Manias, E.; Snyder, A. J.; Runt, J. *Macromolecules* **2001**, *34*, 337−339.
(9) Bharadwaj, R. K. *Macromolecules* **2001**, *34*, 1989−92.
(10) Messersmith, P. B.; Giannelis, E. P. *J. Polym. Sci., Part A: Polym. Chem.* **1995**, *33*, 1047−57.
(11) Yano, K.; Usuki, A.; Okada, A.; Kurauchi, T.; Kamigaito, O. *J. Polym. Sci., Part A: Polym. Chem.* **1993**, *31*, 2493−98.
(12) Deleted in Proof.
(13) Kojima, Y.; Usuki, A.; Kawasumi, M.; Fukushima, T.; Kamigaito, O. *J. Mater. Res.* **1993**, *8*, 1179−84.
(14) (a) Kojima, Y.; Usuki, A.; Kawasumi, M.; Okada, A.; Kurauchi, T.; Kamigaito, O. *J. Polym. Sci., Part A: Polym. Chem.* **1993**, *31*, 983. (b) Kojima, Y.; Usuki, A.; Kawasumi, M.; Okada, A.; Fukushima, Y.; Kurauchi, T.; Kamigaito, O. *J. Mater. Res.* **1993**, *8*, 1185. (c) Kawasumi, M. *J. Polym. Sci., Part A: Polym. Chem.* **2004**, *42*, 819−824.
(15) Gilman, J. W. *Appl. Clay Sci.* **1999**, *15*, 31−49.
(16) Gilman, J. W.; Jackson, C. L.; Morgan, A. B.; Harris, R., Jr.; Manias, E.; Giannelis, E. P.; Wuthenow, M.; Hilton, D.; Phillips, S. H. *Chem. Mater.* **2000**, *12*, 1866−73.
(17) Dabrowski, F.; Bourbigot, S.; Delbel, R.; Bras, M. L. *Eur. Polym. J.* **2000**, *36*, 273−84.
(18) Lan, T.; Kaviratna, P. D.; Pinnavaia, T. J. *Chem. Mater.* **1994**, *6*, 573−575.
(19) Ozin, G. *Adv. Mater.* **1992**, *4*, 612.
(20) Mehnert, C. P.; Ying, J. Y. *Chem. Commun.* **1997**, 2215.
(21) (a) Pinnavaia, T. J. *Science* **1983**, *220*, 365. (b) Lan, T.; Kaviratna, P. D.; Pinnavaia, T. J. *Chem. Mater.* **1995**, *7*, 2144. (c) Solomon, D. H.; Hawthorne, D. G. *Chemistry of Pigments and Fillers*; Wiley: New York, 1983; pp 136−144.
(22) Wei, Y.; Wang, W.; Yang, D.; Tang, L. *Chem. Mater.* **1994**, *6*, 1737.
(23) Carrado, K. A.; Xu, L. *Chem. Mater.* **1998**, *10*, 1440.
(24) (a) Buxton, G. A.; Balazs, A. C. *J. Chem. Phys.* **2002**, *117*, 7649−7658. (b) Zhulina, E.; Singh, C.; Balazs, A. C. *Langmuir* **1999**, *15*, 3935−3943.
(25) Lyatskaya, Y.; Balazs, A. C. *Macromolecules* **1998**, *31*, 6676−6680.
(26) (a) Kawasumi, M.; Hasegawa, N.; Kato, M.; Usuki, A.; Okada, A. *Macromolecules* **1997**, *30*, 6333. (b) Aranda, P.; Ruiz-Hitzky, E. *Chem. Mater.* **1992**, *4*, 1395. (c) Wu, J.; Lerner, M. M. *Chem. Mater.* **1993**, *5*, 835. (d) Sugahara, Y.; Sugiyama, T.; Hagayama, T.; Kuroda, K.; Kato, C. *J. Chem. Soc., Faraday Trans.* **1987**, *83*, 1851. (e) Sellinger, A.; Weiss, P. M.; Nguyen, A.; Lu, Y.; Assink, R. A.; Gong, W.; Brinker, C. J. *Nature (London)* **1998**, *394*, 256.
(27) Krishnamoorti, R.; Giannelis, E. P. *Macromolecules* **1997**, *30*, 4097−4102.
(28) (a) Vaia, R. A.; Giannelis, E. P. *Macromolecules* **1997**, *30*, 8000−8009. (b) Vaia, R. A.; Jandt, K. D.; Kramer, E. J.; Giannelis, E. P. *Macromolecules* **1995**, *28*, 8080−8085.
(29) Alexandre, M.; Dubois, P. *Mater. Sci. Eng.* **2000**, *28*, 1.
(30) Kojima, Y.; Usuki, A.; Kawasumi, M.; Okada, A.; Kurauchi, T.; Kamigaito, O. *J. Polym. Sci., Part A: Polym. Chem.* **1993**, *31*, 1755.
(31) Webster, O. W. *Science* **1991**, *251*, 887.
(32) (a) Ginzburg, V. V.; Balazs, A. C. *Adv. Mater.* **2000**, *12*, 1805−1809. (b) Kuznetsov, D. V.; Balazs, A. C. *J. Chem. Phys.* **2000**, *112*, 4365−4375.
(33) Weimer, M. W.; Chen, H.; Giannelis, E. P.; Sogah, D. Y. *J. Am. Chem. Soc.* **1999**, *121*, 1615−1616.
(34) Fan, X.; Zhou, Q.; Xia, C.; Cristofoli, W.; Mays, J.; Advincula, R. *Langmuir* **2002**, *18*, 4511−4518.
(35) Krishnamoorti, R.; Giannelis, E. P. *Macromolecules* **1997**, *30*, 4097.
(36) Kubies, D.; Pantoustier, N.; Dubois, P.; Rulmont, A.; Jerome, R. *Macromolecules* **2002**, *35*, 3318−3320.
(37) Lepoittevin, B.; Pantoustier, N.; Alexandre, M.; Calberg, C.; Jerome, R.; Dubois, P. *J. Mater. Chem.* **2002**, *12*, 3528−3532.
(38) Lepoittevin, B.; Pantoustier, N.; Devalckenaere, M.; Alexandre, M.; Kubies, D.; Calberg, C.; Jerome, R.; Dubois, P. *Macromolecules* **2002**, *35*, 8385−8390.
(39) Lepoittevin, B.; Pantoustier, N.; Alexandre, M.; Calberg, C.; Jerome, R.; Dubois, P. *Macromol. Symp.* **2002**, *183*, 95−102.
(40) (a) Hawker, C. J. *Acc. Chem. Res.* **1997**, *30*, 373. (b) Puts, R. D.; Sogah, D. Y. *Macromolecules* **1996**, *29*, 3323. (c) Matyjaszewski, K.; Patten, T. E.; Xia, J. *J. Am. Chem. Soc.* **1997**, *119*, 674. (d) Percec, V.; Barboiu, B.; Neumann, A.; Ronda, J. C.; Zhao, M. *Macromolecules* **1996**, *29*, 3665. (e) For a comprehensive review of RAFT, see: Moad, G.; Solomon, D. H. *The Chemistry of Free Radical Polymerization*; Pergamon: Oxford, 1995. (f) For a more recent review, see: Perrier, S.; Takolpuckdee, P. *J. Polym. Sci., Part A: Polym. Chem.* **2005**, *43*, 5347−5393.
(41) (a) Boettcher, H.; Hallensleben, M. L.; Nuss, S.; Wurm, H.; Bauer, J.; Behrens, P. *J. Mater. Chem.* **2002**, *12*, 1351−1354. (b) Zhao, H.; Argoti, S. D.; Farrell, B. P.; Shipp, D. A. *J. Polym. Sci., Part A: Polym. Chem.* **2004**, *42*, 916−924. (c) Zhao, H.; Farrell, B. P.; Shipp, D. A. *Polymer* **2004**, *45*, 4473−4481. (d) Zhao, H.; Shipp, D. A. *Chem. Mater.* **2003**, *15*, 2693−2695. (e) Li, C.-P.; Huang, C.-M.; Hsieh, M.-T.; Wei, K.-H. *J. Polym. Sci., Part A: Polym. Chem.* **2005**, *43*, 534−542.
(42) Salem, N.; Shipp, D. A. *Polymer* **2005**, *46*, 8573−8581.
(43) (a) Otsu, T. *J. Polym. Sci.* **1956**, *21*, 559−561. (b) Otsu, T.; Yoshida, M.; Tazaki, T. *Makromol. Chem., Rapid Commun.* **1982**, *3*, 133−140. (c) Otsu, T.; Kuriyama, A. *J. Macromol. Sci., Chem.* **1984**, *A21*, 961−977. (d) Otsu, T.; Kuriyama, A. *Polym. J.* **1985**, *17*, 97−104.
(44) Rammo, J.; Schneider, H.-J. *Inorg. Chim. Acta* **1996**, *251*, 125−134.
(45) (a) Hertler, W. R.; Sogah, D. Y.; Boettcher, F. P. *Macromolecules* **1990**, *23*, 1264−1268. (b) Prucker, O.; Ruhe, J. *Macromolecules* **1988**, *21*, 592. (c) Meier, L. P.; Shelden, R. A.; Caseri, W. R.; Suter, U. W. *Macromolecules* **1994**, *27*, 1637−1642. (d) Blomberg, S.; Ostberg, S.; Harth, E.; Bosman, A. W.; van Horn, B.; Hawker, C. J. *J. Polym. Sci., Part A: Polym. Chem.* **2002**, *40*, 1309−1320. (e) Luo, N.; Hutchinson, J. B.; Anseth, K. S.; Bowman, C. N. *J. Polym. Sci., Part A: Polym. Chem.* **2002**, *40*, 1885−1891.
(46) Zheng, X.; Wilkie, C. A. *Polym. Degrad. Stab.* **2003**, *82*, 441−450.

MA049794I